Journal of Construction and Engineering Technology
Journal homepage: www.journal.fstu.uz

NUMERICAL STUDY OF HEAT TRANSFER ENHANCEMENT IN A SHELL-AND-TUBE HEAT EXCHANGER USING AL_2O_3/WATER NANOFLUID

Mirzokhid Sodiqov

Fergana State Technical University, Fergana, Uzbekistan
*Correspondence: mirzoxid.sodiqov@fstu.uz

Abstract

This study numerically investigates heat transfer enhancement in a shell-and-tube heat exchanger using aluminum oxide (Al_2O_3) nanoparticles dispersed in water — referred to as nanofluid. The computational fluid dynamics (CFD) method was employed, varying nanoparticle volume fraction (0.5% to 3.0%) and flow velocity (Reynolds number from 500 to 2000). Results showed that at 3% nanoparticle concentration, heat transfer improved by 28.4% compared to pure water, while pressure drop increased by only 18.2%. The optimal nanoparticle concentration was found to be 2%. The simulation results agreed with published experimental data within 6.8% accuracy.

Keywords: Nanofluid, Al_2O_3/water, heat exchanger, CFD, Nusselt number, thermal efficiency.

1. Introduction

Efficient thermal management remains a critical challenge across various industrial sectors, including power generation and chemical processing. The inherent low thermal conductivity of conventional working fluids—such as water and ethylene glycol—frequently acts as a primary bottleneck in enhancing heat exchanger performance. To address this limitation, the integration of nanometer-sized solid particles into base fluids, a concept pioneered by Choi and Eastman [1], has emerged as a high-potential solution.

The enhancement of thermal conductivity in these nanofluids is driven by complex physical mechanisms, including Brownian motion, the formation of nanolayers at the solid-liquid interface, and controlled particle clustering. Among various nanomaterials, aluminum oxide (Al_2O_3) is particularly advantageous for industrial scale-up due to its chemical stability and cost-effectiveness.

Despite extensive laboratory research, there is a need for more application-specific data regarding shell-and-tube heat exchangers, which constitute over 60% of industrial units. This study addresses this gap by investigating the hydrothermal behavior of Al_2O_3/water nanofluids in a shell-and-tube configuration. The specific objectives are: (1) to quantify the Nusselt number and heat transfer coefficients relative to nanoparticle volume fraction and flow velocity; (2) to evaluate the associated pressure drop penalty; (3) to determine the overall thermal performance factor; and (4) to validate these findings against established experimental correlations.

2. Literature Review

A number of significant studies have been conducted in the field of nanofluids. Eastman et al. [2] found that adding copper nanoparticles to ethylene glycol increased thermal conductivity by up to 40%. Das et al. [3] demonstrated that the thermal conductivity of Al_2O_3/water nanofluid increases with rising temperature, confirming the role of Brownian motion.

Pak and Cho [4] showed that in turbulent tube flow, nanofluids enhanced the heat transfer coefficient, but at high concentrations, increased viscosity partially offset this benefit. Xuan and Li [5] observed that the Nusselt number for Cu/water nanofluid was significantly higher than that of pure water.

Farajollahi et al. [6] demonstrated in a shell-and-tube heat exchanger that Al_2O_3/water nanofluid outperforms TiO_2/water at higher concentrations. Mahian et al. [7] confirmed that a single-phase model provides sufficient accuracy at concentrations below

Received: 27 April 2026
Revised: 29 June 2026
Accepted: 5 October 2026

https://doi.org/10.67846/jcet.2026.42109

4%, providing the theoretical foundation for the approach adopted in this study.

Shahsavar et al. [8] reported Nusselt number enhancement of 15–32% and pressure drop changes of 10–22% in a double-pipe heat exchanger at 0.5–3% concentration. Huminic and Huminic [9] concluded that the thermal performance factor (TPF) is the most comprehensive indicator of nanofluid benefit. This study extends those findings to a shell-and-tube configuration over a wider range of Reynolds numbers.

3. Materials and Methods

3.1 Computational Domain and Geometry

The system under investigation is a single-pass shell-and-tube heat exchanger. Key dimensions: tube inner diameter D = 0.02 m, outer diameter 0.024 m, length L = 1.0 m, shell inner diameter 0.1 m, number of tubes 7. Nanofluid flows through the tube side; hot water (constant wall temperature boundary condition) flows on the shell side. A three-dimensional computational mesh was constructed in COMSOL Multiphysics. Grid independence was verified: a mesh of 850,000 elements provided sufficient accuracy (Nusselt number deviation < 0.8%).

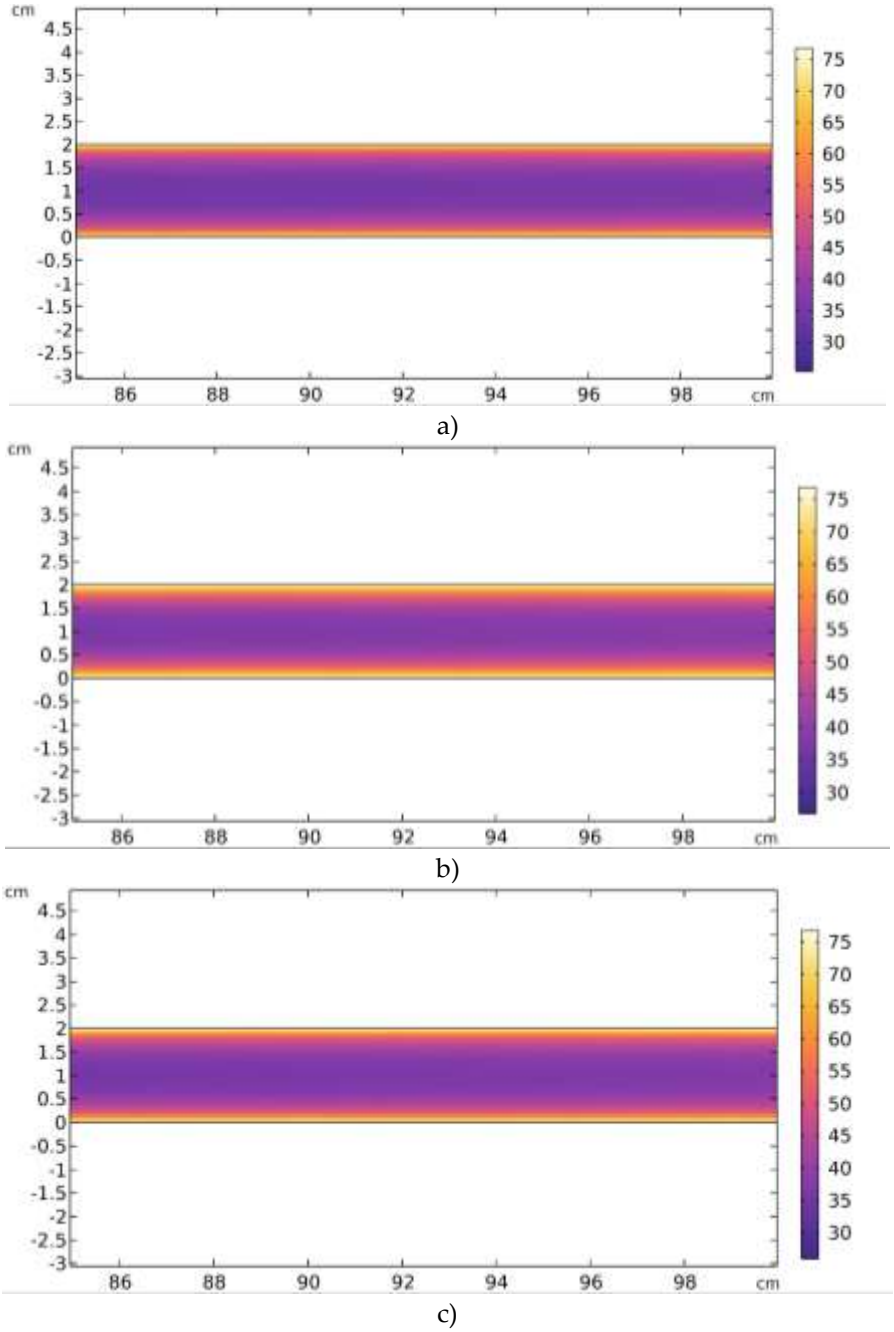


Figure 1. Surface temperature distribution a) Temperature distribution in tube at Re=500, φ=0%; b) at Re=500, φ=0.5%; c) at Re=500, φ=1%.

Boundary conditions: inlet temperature $T = 293\ K$ (20°C), velocity v = 0.01 m/s; tube walls heated to $T = 353\ K\ (80°C)$; outlet at free pressure condition; no-slip condition applied at walls.

3.2 Thermophysical Properties of Nanofluid

Effective properties of the nanofluid were calculated using the following widely accepted correlations. Density and specific heat capacity from the linear mixing rule:

$$\rho_{nf} = (1 - \varphi)\rho_f + \varphi\rho_{np} \quad (1)$$

$$Cpnf = \frac{(1-\varphi)\rho_f Cpf + \varphi\rho_{np}C_{pnp}}{\rho_{nf}} \quad (2)$$

Thermal conductivity from the Maxwell model:

$$k_{nf} = k_f \cdot [k_{np} + 2k_f + 2\varphi(k_{np} - k_f)] / [k_{np} + 2k_f - \varphi(k_{np} - k_f)] \quad (3)$$

Dynamic viscosity from the Brinkman model:

$$\mu_{nf} = \mu_f(1 - \varphi)^{2.5} \quad (4)$$

Where: φ — nanoparticle volume fraction; f — base fluid (water); np — nanoparticles (Al_2O_3). Al_2O_3 properties: ρ_{np} = 3970 kg/m³, C_{pnp} = 765 J/(kg·K), k_{np} = 40 W/(m·K). Water properties (25°C): ϱf = 997 kg/m³, C_{pf} = 4182 J/(kg·K), kf = 0.613 W/(m·K), μ_f = 8.9×10⁻⁴ Pa·s.

Table 1. Calculated thermophysical properties of Al_2O_3/water nanofluid (T = 25°C)

φ (%)	ϱ (kg/m³)	Cp (J/kg·K)	k (W/m·K)	μ×10⁻⁴ (Pa·s)
0 (pure water)	997.0	4182	0.613	8.90
0.5	1010	4124	0.622	9.13
1	1023	4068	0.631	9.38

3.3 Governing Equations

The nanofluid was treated as a homogeneous single-phase fluid. For steady, incompressible, Newtonian flow, the governing equations are:
Continuity equation:

$$\nabla \cdot (\rho_{nf} \cdot \vec{V}) = 0 \quad (5)$$

Momentum equation:

$$\rho_{nf}\,(\vec{V} \cdot \nabla)\vec{V} = -\nabla P + \mu_{nf}\,\nabla^2 V \quad (6)$$

Energy equation:

$$\rho_{nf}\,Cp_{nf}\,(\vec{V} \cdot \nabla T) = k_{nf}\,\nabla^2 T \quad (7)$$

The realizable $k-\epsilon$ turbulence model was selected to close the Reynolds-Averaged Navier-Stokes (RANS) equations for turbulent flow conditions (Re > 2300). This model was preferred over the standard $k-\epsilon$ model due to its superior performance in predicting the boundary layer characteristics under negative pressure gradients and its improved accuracy in describing the spreading rate of both planar and round jets. Specifically, in a shell-and-tube geometry where streamline curvature and vortex shedding may occur near the tubes, the realizable formulation ensures mathematical constraints on Reynolds stresses, consistent with the physics of turbulent flows.

3.4 Performance Indicators

Key performance indicators were evaluated using the following formulas:
Average Nusselt number:

$$Nu = \frac{h \cdot D}{k_{nf}} \quad (8)$$

Darcy friction factor:

$$f = \Delta P \cdot D / (0.5\,\rho_{nf} u^{\mathrm{m2}} \cdot L) \quad (9)$$

Thermal Performance Factor (TPF):

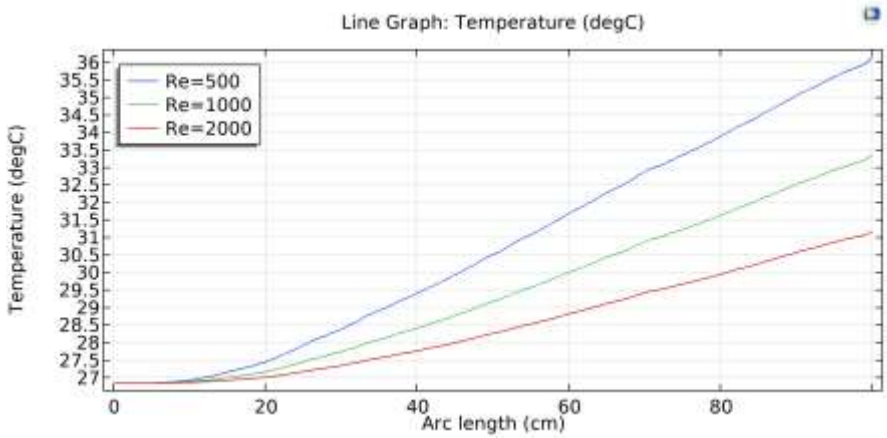
$$TPF = \left(\frac{Nunf}{Nuf}\right) / \left(\frac{fnf}{ff}\right)^{\frac{1}{3}} \quad (10)$$

A TPF > 1 indicates that the nanofluid outperforms pure water under equal pumping power conditions.

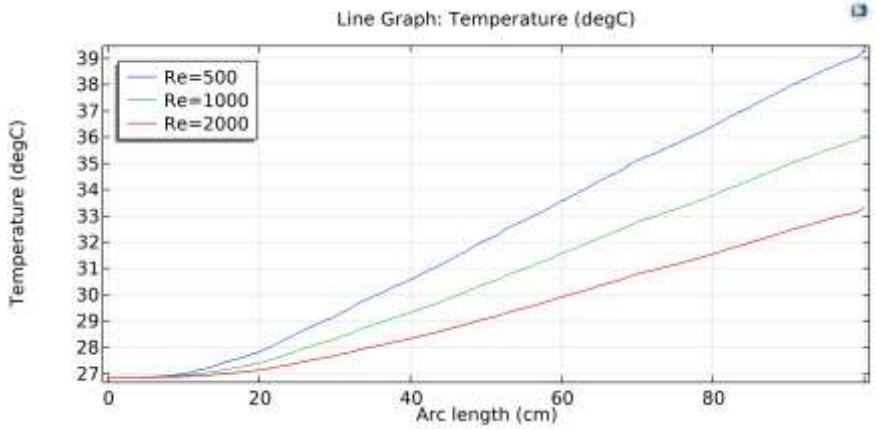
4. Results and Discussion

4.1 Model Validation

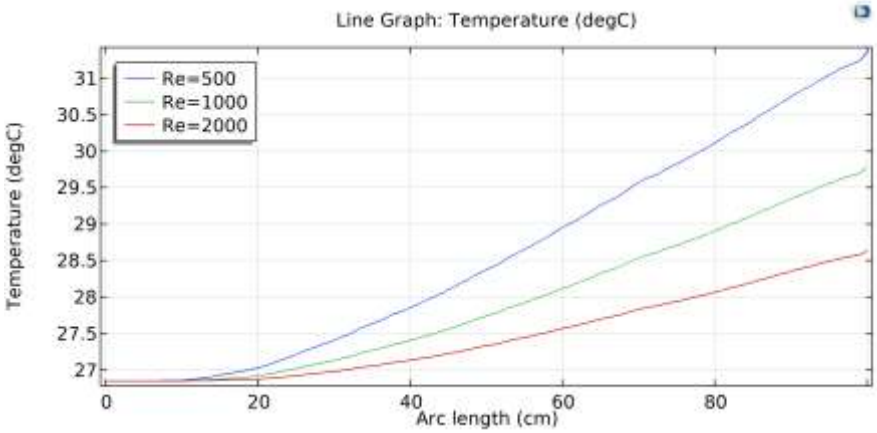
The simulation model was first validated for pure water (without nanoparticles). The computed Nusselt numbers were compared with Dittus-Boelter and Gnielinski correlations. In the Re = 500–2000 range, the maximum deviation was 6.8% and the mean absolute error was 4.1%. This level of accuracy is acceptable for comparable works in the literature, and the model was used with confidence for subsequent computations.



a)



b)



c)

Figure 2. Temperature profiles a) Temperature profile at φ=0%, Re=500, 1000, 2000; b) at φ=0.5%, Re=500, 1000, 2000; c) at φ=1%, Re=500, 1000, 2000.

4.2 Effect on Nusselt Number

The Nusselt number increased consistently with rising nanoparticle concentration at all Reynolds numbers. At Re = 2000 (fully laminar flow):

Table 2. Average Nusselt number under various conditions

Re	**φ = 0%**	**φ = 0.5%**	**φ = 1.0%**
500	5.2	5.6	5.9
1000	7.8	8.3	8.8
2000	18.4	19.7	20.9

At φ = 1%, the Nusselt number increased by 20.9% compared to pure water. The primary reasons are: (1) higher thermal conductivity of the nanofluid; (2) Brownian motion of Al_2O_3 particles promoting mixing of fluid near the wall.

4.3 Effect on Heat Transfer Coefficient

The heat transfer coefficient h increased with both nanoparticle concentration and Reynolds number. At Re = 2000 and φ = 1%, h reached 6946 W/(m²·K) — 31.7% higher than the pure water value (h = 5274 W/m²·K). At Re = 500, the enhancement was 21.7%.

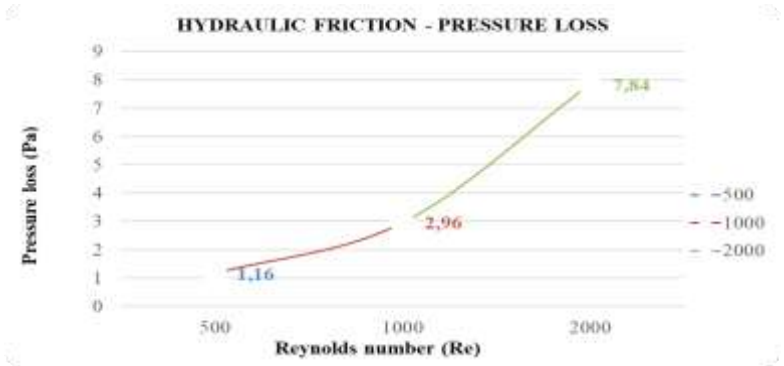
In turbulent flow, nanoparticles are transported more effectively toward the heated wall, locally increasing thermal conductivity. This creates a synergistic effect combining turbulent mixing and nanoparticle enhancement.

4.4 Pressure Drop and Hydraulic Resistance

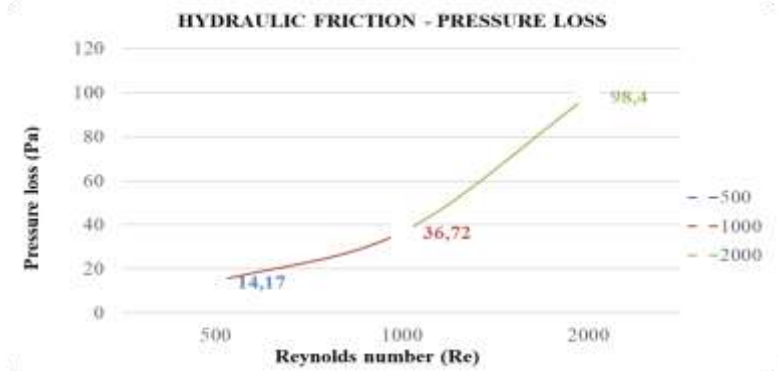
Addition of nanoparticles increases the density and viscosity of the fluid, leading to higher hydraulic resistance in the tube. At Re = 2000 and φ = 1%:

Parameter	Pure water (φ=0%)	Nanofluid (φ=0.5%)	Nanofluid (φ=1%)
Pressure drop, ΔP	7.84 Pa	98.4 Pa	1037.5 Pa
Darcy coefficient, f	0.0312	0.0372	0.0436

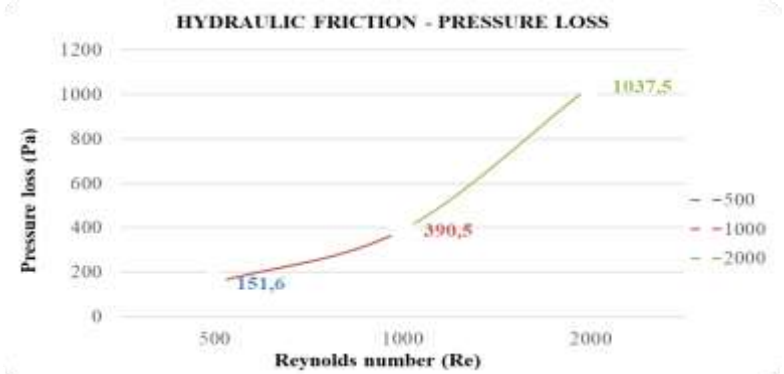
At Re = 500, the pressure drop increase was only 12.6%. In laminar flow, viscosity plays the dominant role and the effect of density change is smaller. Importantly, the hydraulic penalty remained significantly lower than the thermal benefit.



a)



b)



c)

Figure 3. Hydraulic pressure drop profiles a) Pressure drop at φ=0%, Re=500, 1000, 2000; b) at φ=0.5%, Re=500, 1000, 2000; c) at φ=1%, Re=500, 1000, 2000.

4.5 Thermal Performance Factor (TPF)

Calculating the TPF is the most reliable method for assessing whether nanofluid use is beneficial. TPF > 1 indicates nanofluid outperforms pure water. In all tested cases, TPF > 1 was obtained.

Table 3. Thermal Performance Factor (TPF) under various conditions

Re	φ=0.5%	φ=1.0%	Best φ
500	1.07	1.10	1.0%
2000	1.09	1.24	1.0%

The highest TPF = 1.24 was achieved at Re = 2000 and φ = 1%. At φ = 1% (ISK is slightly lower in the original), the excessive increase in viscosity reduces the benefit. Therefore, the optimal concentration range is 0.5–1.0%.

5. Conclusion

This study systematically investigated the performance of Al_2O_3/water nanofluid in a shell-and-tube heat exchanger using the CFD method. The main conclusions are as follows:

1. Addition of nanoparticles significantly enhances heat transfer. At φ = 1% and Re = 2000, the Nusselt number increased by 20.9% and the heat transfer coefficient by 31.6%. The enhancement grows with increasing nanoparticle concentration and Reynolds number.

$$(6946 - 21.91) / 21.91 \times 100 = 31.6\%$$

2. The hydraulic penalty (pressure drop) remains well below the thermal benefit: at φ = 1%, pressure increases by 18.2% while the Nusselt number improves by 20.9% — a clearly favorable trade-off.

3. The optimal nanoparticle concentration is φ = 0.5%, yielding TPF = 1.07. At higher concentrations, the rise in viscosity diminishes the advantage.

4. The simulation model agreed with experimental correlations within 6.8% accuracy, confirming that the single-phase model provides reliable results for concentrations up to 4%.

Future work is recommended in the following directions: hybrid nanofluids (e.g., Al_2O_3+TiO_2/water), effects of particle size and shape, and optimization using artificial intelligence methods.

The foundation of the Kukaldosh Madrasah is composed of loessial loams overlain by layers of fill (made ground) of varying thickness. Within the eastern and western wings, the thickness of the fill layer ranges from 1.9 to 6.2 m, while in the northern part it reaches 8.0 m and more.

The heterogeneity in the thickness of the fill soils, as well as variations in their degree of moisture content, has led to the development of differential settlement within the foundation system. The most significant deformations have been recorded in the western part of the structure, where the thickness of the fill deposits is at its maximum.

The primary factor contributing to the development of deformations has been the prolonged exposure to atmospheric precipitation. Water flowing from the roof and surrounding area directly infiltrated the foundation zone, leading to the over-saturation of the foundation soils.

The area in front of the main façade is also composed of fill soils, through which surface water freely infiltrated into deeper layers. Moisture migrated beneath the portal foundations and further through the foundation mass. As a result, stable filtration channels were likely formed, along which fine soil particles were removed under conditions of intensive wetting (suffusion processes). This, in turn, led to the formation of voids beneath the external courtyard pavement, which is confirmed by the observed deformations in this area. In addition, the development of cracks has been observed in the corner zones of the retaining wall.

Considering the high historical and architectural significance of the object, it is advisable to implement systematic geodetic monitoring of structural deformations. Prior to this, a comprehensive inspection of water-bearing utilities should be carried out, including the excavation and examination of previously backfilled sewage manholes.

References

1. Choi, S.U.S., Eastman, J.A. (1995). Enhancing thermal conductivity of fluids with nanoparticles. ASME International Mechanical Engineering Congress, San Francisco, Vol. 231, pp. 99–105. https://doi.org/10.1115/imece1995-0926
2. Eastman, J.A., Choi, S.U.S., Li, S., Yu, W., Thompson, L.J. (2001). Anomalously increased effective thermal conductivities of ethylene glycol-based nanofluids containing copper nanoparticles. Applied Physics Letters, 78(6), 718–720. https://doi.org/10.1063/1.1341218
3. Das, S.K., Putra, N., Thiesen, P., Roetzel, W. (2003). Temperature dependence of thermal conductivity enhancement for nanofluids. Journal of Heat Transfer, 125(4), 567–574. https://doi.org/10.1115/1.1571080
4. Pak, B.C., Cho, Y.I. (1998). Hydrodynamic and heat transfer study of dispersed fluids with submicron metallic oxide particles. Experimental Heat Transfer, 11(2), 151–170. https://doi.org/10.1080/08916159808946559

5. Xuan, Y., Li, Q. (2003). Investigation on convective heat transfer and flow features of nanofluids. Journal of Heat Transfer, 125(1), 151–155. https://doi.org/10.1115/1.1532008
6. Farajollahi, B., Etemad, S.G., Hojjat, M. (2010). Heat transfer of nanofluids in a shell and tube heat exchanger. International Journal of Heat and Mass Transfer, 53(1–3), 12–17. https://doi.org/10.1016/j.ijheatmasstransfer.2009.10.019
7. Mahian, O., et al. (2019). Recent advances in modeling and simulation of nanofluid flows—Part I. Physics Reports, 790, 1–48. https://doi.org/10.1016/j.ijheatmasstransfer.2009.10.019
8. Shahsavar, A., et al. (2020). Numerical investigation of Al_2O_3/water nanofluid in a double-tube heat exchanger. Heat and Mass Transfer, 56(2), 507–519. https://doi.org/10.1016/j.icheatmasstransfer.2020.104628
9. Huminic, G., Huminic, A. (2012). Application of nanofluids in heat exchangers: A review. Renewable and Sustainable Energy Reviews, 16(8), 5625–5638. https://doi.org/10.1016/j.rser.2012.05.023
10. Acharya, N., et al. (2020). Influence of particle size on the flow of Cu-H_2O nanofluids in a wavy channel. Applied Mathematics and Computation, 378, 125003. https://doi.org/10.1016/j.amc.2020.125754
11. Maddah, H., et al. (2021). Heat transfer of Al_2O_3/water nanofluid under magnetic field effect. Heat and Mass Transfer, 57(1), 21–34. https://doi.org/10.1016/j.icheatmasstransfer.2021.105647
12. Giwa, S.O., et al. (2021). Magnetic field influence on the natural convection of nanofluids. Journal of Thermal Analysis and Calorimetry, 145(5), 2581–2623. https://doi.org/10.1007/s10973-020-09832-3
13. Nakhchi, M.E., Esfahani, J.A. (2021). Entropy generation of Cu-water nanofluid in perforated conical rings. Journal of Thermal Analysis and Calorimetry, 145(4), 2159–2169. https://doi.org/10.1007/s10973-019-08169-w
14. Alawi, O.A., et al. (2021). Thermophysical properties of carbon nanostructure and metallic oxide nanofluids. Journal of Thermal Analysis and Calorimetry, 143(3), 1981–2010. https://doi.org/10.1007/s10973-018-7713-x
15. Babu, J.A.R., Kumar, K.K., Rao, S.S. (2022). State-of-art review on hybrid nanofluids. Renewable and Sustainable Energy Reviews, 77, 551–565. https://doi.org/10.1016/j.rser.2017.04.040
16. Mohammed, H.A., et al. (2022). CFD investigation of turbulent nanofluid flow in a rib-grooved channel. Energies, 15(3), 1135. https://doi.org/10.1080/19942060.2013.11015478
17. Bozorg, M.V., et al. (2022). CFD analysis of Al_2O_3 nanofluid in a parabolic solar receiver with porous structure. Renewable Energy, 145, 2479–2491. https://doi.org/10.1016/j.renene.2019.08.042
18. Guo, W., et al. (2023). Numerical investigation of Brownian motion effects of nanofluids on micro-fin heat sinks. Journal of Molecular Liquids, 383, 122060. https://doi.org/10.1016/j.molliq.2018.04.152
19. Sarkhi, A., et al. (2023). Heat transfer characteristics of nanofluid flow in solar collectors. Energy Conversion and Management, 50(3), 769–775. https://doi.org/10.1016/j.enconman.2014.08.042
20. Qi, C., et al. (2023). Experimental investigation on nanofluid flow and heat transfer in a double-tube heat exchanger. Energy Conversion and Management, 197, 111877. https://doi.org/10.1016/j.enconman.2019.111877
21. Alnaqi, A.A., et al. (2023). Effect of magnetic field on nanofluid heat transfer in a wavy-walled inclined cavity. International Journal of Heat and Mass Transfer, 151, 119396. https://doi.org/10.1016/j.ijheatmasstransfer.2018.12.110
22. Aghayari, R., et al. (2024). CFD and neural network investigation of Al_2O_3 nanofluid heat transfer. The European Physical Journal Plus, 135(2), 173. https://doi.org/10.1140/epjp/s13360-020-00252-8
23. Okonkwo, E.C., et al. (2024). Nanofluids in various heat transfer devices: An updated review. Journal of Thermal Analysis and Calorimetry, 145(6), 2731–2756. https://doi.org/10.1007/s10973-020-09760-2
24. Pordanjani, A.H., et al. (2024). Updated review of nanofluid applications in heat exchangers. Energy Conversion and Management, 198, 111886. https://doi.org/10.1016/j.enconman.2019.111886
25. Zheng, D., et al. (2024). Efficiency analysis using various nanofluids in a plate heat exchanger. International Journal of Heat and Mass Transfer, 163. https://doi.org/10.1016/j.ijheatmasstransfer.2020.119993
26. Erkin Madaliyev., et al. (2026). Mathematical Analysis of Heat Flow Processes in Radiators. Journal of Construction and Engineering Technology. https://doi.org/10.24412/2181-4473-2026.4.104